JVI Journals.ASM.org

Clustering and Mobility of HIV-1 Env at Viral Assembly Sites Predict Its Propensity To Induce Cell-Cell Fusion

Nathan H. Roy,[a] Jany Chan,[b] Marie Lambelé,[b] Markus Thali[a,b,c]

Graduate Program in Cell and Molecular Biology,[a] Department of Microbiology and Molecular Genetics,[b] and College of Medicine and CALS,[c] University of Vermont, Burlington, Vermont, USA

HIV-1 Env mediates virus attachment to and fusion with target cell membranes, and yet, while Env is still situated at the plasma membrane of the producer cell and before its incorporation into newly formed particles, Env already interacts with the viral receptor CD4 on target cells, thus enabling the formation of transient cell contacts that facilitate the transmission of viral particles. During this first encounter with the receptor, Env must not induce membrane fusion, as this would prevent the producer cell and the target cell from separating upon virus transmission, but how Env's fusion activity is controlled remains unclear. To gain a better understanding of the Env regulation that precedes viral transmission, we examined the nanoscale organization of Env at the surface of producer cells. Utilizing superresolution microscopy (stochastic optical reconstruction microscopy [STORM]) and fluorescence recovery after photobleaching (FRAP), we quantitatively assessed the clustering and dynamics of Env upon its arrival at the plasma membrane. We found that Gag assembly induced the aggregation of small Env clusters into larger domains and that these domains were completely immobile. Truncation of the cytoplasmic tail (CT) of Env abrogated Gag's ability to induce Env clustering and restored Env mobility at assembly sites, both of which correlated with increased Env-induced fusion of infected and uninfected cells. Hence, while Env trapping by Gag secures Env incorporation into viral particles, Env clustering and its sequestration at assembly sites likely also leads to the repression of its fusion function, and thus, by preventing the formation of syncytia, Gag helps to secure efficient transfer of viral particles to target cells.

The envelope glycoprotein (Env) of human immunodeficiency virus type 1 (HIV-1) (and other retroviruses) mediates the attachment of viral particles to target cells and the subsequent fusion of viral and cellular membranes (1). These processes, by definition, mark the beginning of the early phase of the viral replication cycle. Env functions are thus critical during virus entry, and yet, Env is also required during the late phase of the viral replication cycle: while still situated at the plasma membrane of infected cells, Env triggers the formation of the virological synapse (VS), a distinct cell alignment that secures the efficient spread of HIV-1 and other viruses (2, 3). Already two decades ago, evidence began to emerge which suggested that HIV-1 transmission occurs most efficiently when infected cells adhere to uninfected cells (4–7). That these (often transient) contacts are indeed sites of particle transmission was later visualized and confirmed in tissue culture (8–12). More recently, an intravital imaging analysis of HIV-1-infected humanized mice showed that infected T cells form contacts with uninfected cells, and when the frequency of these contacts was reduced by inhibiting the mobility of the lymphocytes, plasma viremia was significantly decreased, strongly suggesting a role for transient lymphocyte contacts in systemic viral spread *in vivo* (13).

Successful transmission from an infected producer cell to an uninfected target cell requires that the late and early functions of Env are tightly regulated. When still part of the producer cell, i.e., during the late phase of the replication cycle, Env needs to initiate the formation of the VS by engaging the viral receptor CD4 on the target cell (9). Env engagement of the receptor at this point must not lead to fusion of cellular membranes (which would lead to the formation of a syncytium), in order to allow the infected cell to continue contacting uninfected cells to promote viral spread. Once a VS is formed, however, some Env gets incorporated into newly formed viral particles, and as part of these particles, Env again contacts CD4 to mediate the attachment of virions to the target cell. During this second encounter with the viral receptor, at the beginning of the early phase of the viral life cycle, Env needs to mediate the fusion of viral and target cell membranes to allow the viral genome to enter the cytoplasm.

The regulation of Env fusogenicity is linked to the maturation status of Gag: as established by the Aiken and Freed groups, Env becomes fusogenic only after particles have been released and undergone proteolytic maturation (14–16; reviewed in reference 17). Visualizing Env in virions by using superresolution microscopy, a recent study compared the distribution of Env in immature versus mature virions, along with the ability of Env to polarize toward CD4 in target cell membranes (18). The study demonstrated that Env's polarization toward CD4 correlated with Env-induced viral fusion. This, along with a previous electron tomography study of HIV and simian immunodeficiency virus (SIV) virions, which also documented that Env trimers accumulate toward the target cell (forming the "claw" [19]), suggests that Gag maturation-dependent Env mobility is essential for its (polarized) accumulation, which in turn is a prerequisite for Env's ability to fuse viral and cellular membranes.

Gag not only regulates the fusogenicity of Env in virions but is also essential for Env incorporation into the nascent budding particles. Env incorporation is thought to be an active process. It is blocked by distinct mutations and deletions in the membrane

Received 22 March 2013 Accepted 19 April 2013
Published ahead of print 1 May 2013
Address correspondence to Markus Thali, markus.thali@uvm.edu.
Copyright © 2013, American Society for Microbiology. All Rights Reserved.
doi:10.1128/JVI.00790-13

binding matrix (MA) domain of Gag or by small truncations in the long cytoplasmic tail (CT) of Env (20–27; reviewed in reference 28). Interestingly, while these studies strongly suggest that direct or indirect interactions between Env and Gag mediate Env incorporation into viral particles, deletion of the whole cytoplasmic tail of Env (ΔCT) can overcome many of the incorporation defects imposed by mutations in MA, at least in some cell types (23, 24, 29, 30). These data, along with the observations that retroviruses can incorporate glycoproteins from many other viruses, suggest that there are other forces that contribute to Env incorporation (31). It has been hypothesized (32), for instance, that Gag accumulation at the plasma membrane creates a micromilieu that leads to trapping of Env at future budding sites, similar to the manner in which HIV-1 Gag assembly has been shown to rearrange and trap specific host cell components (33, 34; reviewed in references 35 and 36).

The spatial and temporal aspects of HIV-1 Gag assembly at the plasma membrane have been investigated using live-cell microscopy techniques, such as FRAP (fluorescence recovery after photobleaching) and TIRF (total internal reflection fluorescence) microscopy (37–39). More recently, such studies have been extended to analyze the dynamics of viral RNA-Gag interactions and the recruitment of individual ESCRT components to the sites of assembly (40–43). With the advent of superresolution microscopy, it became possible to examine viral processes unhindered by the diffraction limit. The initial studies using PALM (photoactivated localization microscopy) documented Gag puncta at the plasma membrane (44), while more-recent analyses focused on HIV-1 entry and trafficking (45, 46) and HIV-1 Gag assembly (47–51) and revealed the localization of the restriction factor tetherin relative to Gag and Env (52). Finally, a very recent study, which provided subdiffraction mapping of Gag and Env at the plasma membrane (53), along with elegant correlative electron/fluorescence microscopy (54, 55), addresses the specificity of Env recruitment and its incorporation into budding particles. Although these studies yielded very valuable information, they were not designed to dynamically examine Gag-Env interactions.

Here, we set out to investigate, quantitatively and at the nanoscale level, how Gag engages Env at the plasma membrane of HIV-1-producing cells. Using the superresolution technique called stochastic optical reconstruction microscopy (STORM) and FRAP, we analyzed the role of the Env CT in determining the size and mobility of Env clusters relative to areas of Gag accumulation on the plasma membrane. Collectively, our results provide a nondiffraction-limited quantification of the clustering of Env at HIV-1 assembly sites. Our data also reveal that Gag assembly at the surface of infected cells regulates not only Env distribution but also Env mobility, in an Env CT-dependent manner, likely not only to secure Env incorporation into nascent particles but also to prevent the premature activation of Env fusogenicity and, thus, to avoid the formation of syncytia.

MATERIALS AND METHODS

Cells, plasmids, and antibodies. HeLa cells were maintained in Dulbecco's modified Eagle's medium (DMEM) (MediaTech) supplemented with 10% fetal bovine serum (FBS; Invitrogen). CEMss cells were maintained in RPMI (MediaTech) supplemented with 10% FBS (Invitrogen). We used five proviral constructs: pNL4-3, pNL4-3 ΔCT (a kind gift from Eric Freed), E-I- MA/p6 (a kind gift from Michael Kay), and pNL4-3 iGFP (interdomain green fluorescent protein) and pNL4-3 iGFP ΔCT (provided by Benjamin Chen) (56). E-I- MA/p6 is a pNL4-3-based provirus that has *luc* in the place of *env*, mutations of 5 protease sites in *gag*, and a D116G mutation in *int*. GagGFP and monomeric Gag tagged with the fluorescent protein cerulean (monomeric Gag-cerulean) (57) were both kindly provided by Paul Spearman. Gag-mCherry was a kind gift from Paul Bieniasz. The pCMV-driven clade B wild-type (WT) and ΔCT Env plasmids were kindly provided by Marc Johnson. The following reagent was obtained through the NIH AIDS Research and Reference Reagent Program, Division of AIDS, NIAID, NIH: HIV-1 gp120 monoclonal antibody (2G12) from Hermann Katinger. The anti-CD9 antibody K41 was purchased from Bachem. The 2G12 Fab and K41 Fab were created using the Pierce Fab micropreparation kit following the manufacturer's instructions. The Fab preparation was run on SDS-PAGE and verified by Coomassie staining. Alexa Fluor 647-conjugated secondary antibody was purchased from Molecular Probes, while Fab-Alexa Fluor 488 and Fab-Dylight 594 were purchased from Jackson.

STORM imaging and analysis. Thirty thousand HeLa cells were plated on MatTek dishes (MatTek Corp.). Cells were transfected 24 h later with pNL4-3 or pNL4-3 ΔCT proviral constructs, along with 1/20 Gag-GFP, using Lipofectamine 2000 (following the manufacturer's instructions). Sixteen to 20 h posttransfection, the cells were incubated on ice and labeled with 2G12, fixed with 4% paraformaldehyde (PFA), and probed with anti-human Alexa 647-conjugated antibody (Molecular Probes). Imaging was performed at the UVM Microscopy Imaging Facility on a Nikon N-STORM setup centered around a Nikon Eclipse Ti microscope base. For wide-field images, a Lumencor SOLA light engine was used. For STORM, a 150-mW, 647-nm laser was operated in TIRF mode on continuous illumination. The imaging buffer composition was 50 mM Tris-HCl, 10 mM NaCl, 10% glucose, and 0.1 M cysteamine (Sigma). The buffer was supplemented with an enzymatic oxygen-scavenging system using glucose oxidase (Sigma) and catalase (Sigma). Fifteen thousand to 25,000 frames were collected per image using a 100× PlanApo 1.45NA Nikon objective, with an Andor iXon DU897 electron-multiplying charge-coupled device (EMCCD) camera, at a frame rate of 45 to 60 Hz. Single-molecule fitting and image rendering were performed with the N-STORM software in NIS Elements (version AR 4.00.07), with a localization precision of 25 nm or better (based on a filter for number of photons collected per localization). Image analysis on HeLa cells was done by exporting localization coordinates of 2-μm by 2-μm fields and importing them into MatLab. Once in MatLab, Ripley's K function was calculated and subsequently normalized to $L(r)$, where r is the radius, using the equation $L(r) = \mathrm{sqrt}[K(r)/\pi]$. Plotting $L(r) - r$ [called $H(r)$] versus r allowed the peak of maximum clustering to be determined and represents a number between the radius and diameter of the clusters (58). Although some caveats have been pointed out on the use of Ripley's for estimating domain size (59), these caveats generally involve Ripley's predicting a slightly clustered pattern over large distances even of randomly distributed points (due to overcounting). Because our data show clear, discernible $H(r)$ peaks in the predicted range, we find that our analysis yields useful information to compare cluster size. Also, it is important to note that Ripley's K is also slightly sensitive to the actual density of the individual clusters (also described in reference 50). For example, if similar-sized clusters are further apart, Ripley's will artificially predict a marginally larger value. The only condition where this might come into play is for WT Env clusters outside budding sites, which seem to be a little more dispersed. Interestingly, this would result in a larger average Ripley's value for that condition, but the fact that this is the very condition that yields the smallest average value supports the conclusion that these clusters are indeed smaller. Also, antibody-induced clustering may contribute to Env cluster size, although in the results presented here, we can clearly differentiate different-sized clusters, suggesting that antibody-induced artifacts contribute only to a small degree (as documented in reference 53). For each condition, we used a minimum of 12 total fields from 6 cells over 3 separate imaging sessions. Statistical analysis of $H(r)$ maximums was carried out in GraphPad Prism 5 using a one-way analysis of variance

(ANOVA) with a Bonferroni *post hoc* test. Values were considered significantly different with a P value of ≤ 0.05.

For STORM on CEMss cells, the cells were infected with NL4-3 iGFP and NL4-3 iGFP ΔCT virus (see "Cell-cell fusion assay" below). Forty-eight hours later, the cells were plated on poly-lysine-coated MatTek dishes for 2 h at 37°C and then incubated on ice and labeled with 2G12, fixed with 4% paraformaldehyde (PFA), and probed with anti-human Alexa Fluor 647-conjugated antibody. Before imaging of CEMss cells, dark red FluoSpheres (Molecular Probes) were added as fiducial markers to aid in lateral drift correction during the imaging session. Imaging was performed as described above. For quantification of CEMss cell STORM data, individual budding sites were binned into pixels (px) of 3.69 nm/px and imported into FIJI. Individual budding sites were then fit with a Gaussian distribution, and the full width at half maximum (FWHM) was calculated using FIJI. Statistical analysis was carried out in GraphPad Prism 5 using Student's t test. Values were considered significantly different with a P value of ≤ 0.05.

Cell-cell fusion assay. NL4-3 iGFP and NL4-3 iGFP ΔCT were produced by transfecting 293T cells with pNL4-3 iGFP or pNL4-3 iGFP ΔCT along with vesicular stomatitis virus G glycoprotein (VSV-G) at a 10:1 ratio in a 10-cm plate using the calcium phosphate transfection kit (Invitrogen). At 12 h posttransfection, the medium was replaced, and 24 h later, the supernatant was collected, prespun at $1,000 \times g$ for 10 min, aliquoted, and frozen at −80°C. Viral preparations were used to infect CEMss cells at various dilutions until the conditions yielding similar surface Env levels were identified. To assess Env levels, 48 h after infection, cells were washed, incubated on ice and labeled with 2G12, fixed, probed with secondary Alexa Fluor 647-conjugated antibody, and analyzed on a BD LSRII flow cytometer. iGFP or iGFP ΔCT virus-infected CEMss cells with equal Env levels were then mixed at a 1:3 ratio with 7-amino-4-chloromethylcoumarin (CMAC) (Molecular Probes)-labeled CEMss target cells (staining done according to the manufacturer's protocol). Following a 3-h incubation at 37° with 5% CO_2, the cells were fixed (4% PFA) and plated on poly-lysine-coated MatTek dishes. Multiple fields were imaged using a Nikon Eclipse Ti-E equipped with a Nikon 40× 0.75NA Plan Fluor objective, a Qimaging EXi Blue camera, and NIS Elements software version 3.10. Syncytia were counted as Gag-expressing (green) CEMss cells that were also positive for CMAC. Three independent experiments were carried out, with at least 100 infected cells analyzed per condition per experiment. Statistical analysis was carried out in GraphPad Prism using Student's t test. Values were considered significantly different with a P value of ≤ 0.05.

FRAP imaging and analysis. HeLa cells were plated on MatTek dishes (MatTek Corp.) and transfected 24 h later with E-I- MA/p6, WT or ΔCT Env, and Gag mCherry (ratio, 2:1:1). ΔCT Env was also transfected alone or with monomeric Gag-cerulean. Sixteen to 20 h posttransfection, the cells were incubated on ice and labeled with Fab 2G12, followed by Fab-Alexa Fluor 488 (Jackson ImmunoResearch). The imaging buffer was composed of Hanks' balanced salt solution (HBSS) plus HEPES, and imaging was performed on a Zeiss LSM 510 Meta confocal microscope at the University of Vermont Microscopy Imaging Facility. A 100× PlanApo 1.4NA objective was used, along with a heated stage to keep the cells at 37°C during image acquisition. The imaging time per dish did not exceeded 40 min. FRAP experiments were performed using an argon 488-nm laser line, while before FRAP acquisition, Gag mCherry and monomeric Gag-cerulean were excited with a 543-nm laser and a 458-nm laser, respectively. To control for potential cerulean fluorescence produced by the 488-nm laser, a series of images were acquired, and bleed through of excited cerulean under FRAP conditions was analyzed. Between 1 and 2% fluorescence was observed above background, and thus, we deemed monomeric Gag-cerulean acceptable for our study. Bleaching was done using the argon 488-nm laser at full power for 50 iterations in a circular area of 10.6 μm^2. Cells were then monitored every 10 s for 140 s. All of the images acquired during the bleaching experiments were performed on the basolateral side of cells using one z-section.

FRAP analysis was conducted essentially as described in reference 33. Briefly, Zeiss LSM software was used to obtain intensity values over time in the bleached area, a nonbleached area of the same cell, and an area devoid of cells (background). The bleached-area intensity was converted into fractional recovery and normalized to the unbleached-area intensity of the cell (60). The data were then imported into GraphPad Prism and fitted to the nonlinear regression $Y = \text{span} \times \exp(-K \times X) + \text{plateau}$ (with a half time to recovery $[t_{1/2}]$ of $0.69/K$, where K is the rate constant). Using this regression, we calculated the mobile fraction. The diffusion coefficient (D) was calculated using a simple 2-dimensional model for a circular bleach area $[D = 0.224(r^2/t_{1/2})]$ (61, 62). This analysis was done for each cell (11 total cells per condition, over a total of 6 imaging sessions), and these values were averaged to calculate the mean mobile fraction and mean D. For average recovery curves, each intensity value per cell over time was averaged and plotted. Statistical analysis of the mobile fraction and diffusion coefficient values was carried out in GraphPad Prism using a one-way ANOVA with a Bonferroni *post hoc* test. Values were considered significantly different with a P value of ≤ 0.05.

RESULTS

Nanoscale organization of Env at the surface of HIV-1-expressing cells. Fluorescence microscopy studies were instrumental in revealing where viral components gather for the formation of progeny virions. Recently, superresolution techniques have allowed the visualization and quantification of protein and lipid organization below the diffraction limit (e.g., see references 63–74). Here, we first used STORM to evaluate how Gag assembly regulates the surface distribution of Env. To visualize the viral budding sites, an HIV-1 proviral construct (pNL4-3) was transfected into HeLa cells along with a small amount of a Gag-GFP expression plasmid. Sixteen to 20 h posttransfection, the cells were surface labeled for Env, fixed, labeled with secondary antibody, and imaged as described in Materials and Methods. While discrete clusters of Env could be seen throughout the plasma membrane, most of them gathered at Gag assembly sites (Fig. 1A).

To quantify the observed clustering, we utilized Ripley's K function (75, 76). Ripley's K analysis allows for the preservation of the coordinate-based nature of STORM data. In short, Ripley's K function draws concentric circles around each data point and compares the number of encircled points in the data set to the number of points that would be predicted to lie within the circle if all the points were randomly distributed, thus providing information about whether the data points correspond to a random, clustered, or dispersed pattern. Using a normalized Ripley's function, $H(r)$, the "clustering peak" can then be determined. The $H(r)$ peak corresponds not to the radius of the clusters but to a value that lies between the radius and diameter of the clusters (58; also see Materials and Methods). Our data showed clear peaks of clustering, and WT Env was calculated to have an average $H(r)$ peak of 78 ± 5.4 (Fig. 1C). This $H(r)$ value can be extrapolated to cluster sizes with a diameter of ~105 nm, in agreement with what is shown in the images (Fig. 1A). As the size and the distribution of these clusters were similar to what has been determined by electron microscopy studies for budding HIV-1 virions (for example, see reference 55), they likely represent individual sites of particle assembly. This notion is further supported by the finding that WT Env clusters that were situated at plasma membrane areas where Gag did not assemble were significantly smaller than those at Gag assembly sites, with an average $H(r)$ peak of 48 ± 1.9 (Fig. 1C, compare first 2 bars), corresponding to a cluster diameter of ~65 nm. The results presented in Figure 1 demonstrate that Gag as-

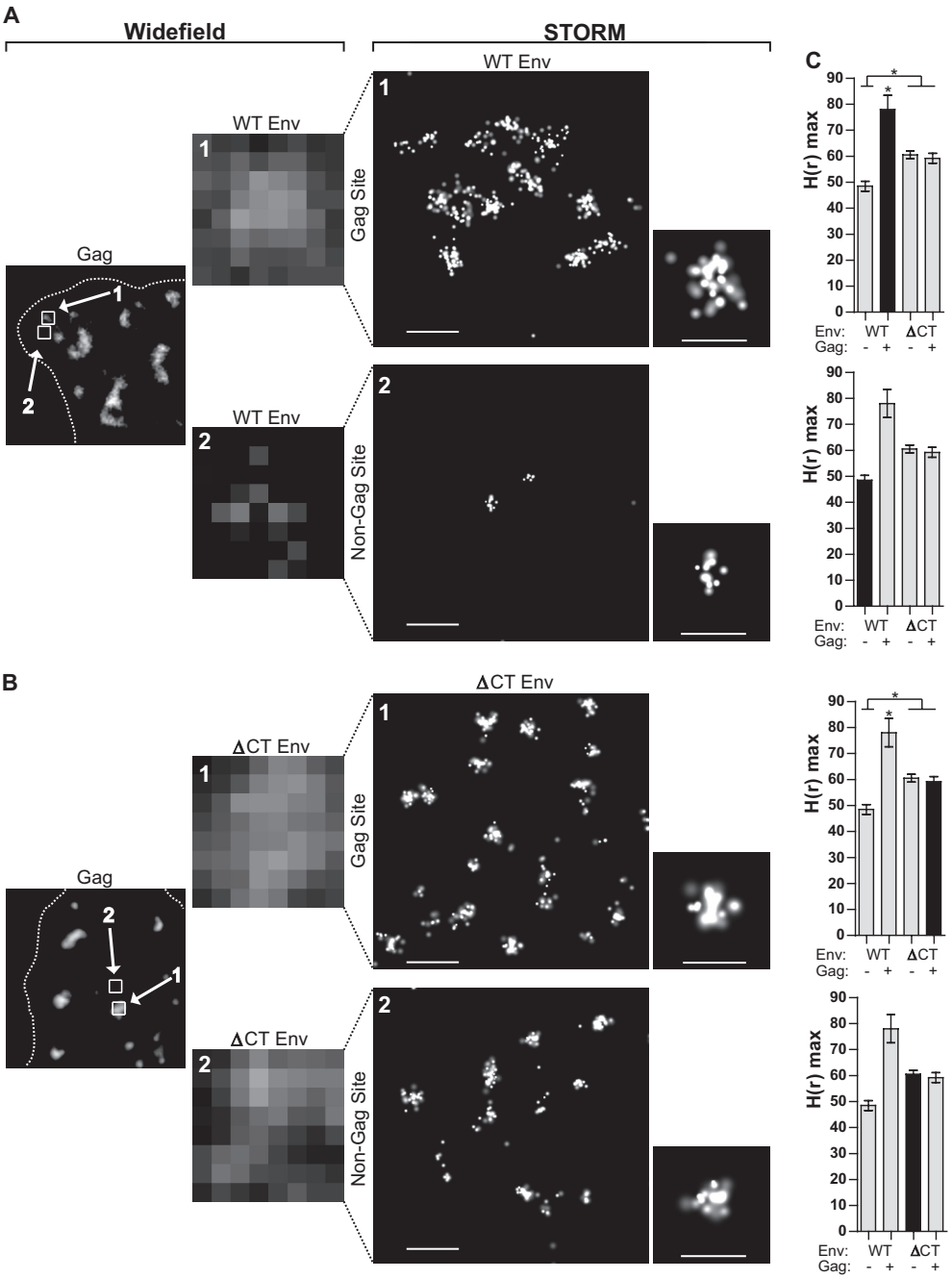

FIG 1 STORM imaging of WT and ΔCT Env in HIV-1-expressing cells. (A, B) HeLa cells expressing pNL4-3 (A) or pNL4-3 ΔCT (B) were subjected to STORM imaging. Boxes labeled 1 and 2 correspond to Gag sites or non-Gag sites, respectively. Scale bars of initial boxes 1 and 2 are 200 nm, while scale bars of the single-cluster blowups represent 100 nm. (C) Quantification of normalized Ripley's *K* peaks. Data are averages from a total of at least 12 2-μm by 2-μm fields of at least six different cells collected from three separate imaging sessions (±standard error of the mean [SEM]). For statistical analysis, a one-way ANOVA was performed with a Bonferroni *post hoc* test. Values were considered significantly different if the *P* value was ≤0.05.

sembly at the plasma membrane results in the aggregation of Env clusters at these sites.

For comparison, we also transfected HeLa cells with a proviral construct that leads to the expression of Env lacking its cytoplasmic tail (pNL4-3 ΔCT) and subjected them to STORM imaging. From diffraction-limited microscopy analyses, we already knew that ΔCT Env, whether expressed alone or in the context of the full virus, has a different staining pattern than WT Env, consistent with the fact that it lacks the multiple trafficking signals harbored in the cytoplasmic domain (77–82; also data not shown). Figure 1B documents that, unlike WT Env, which mainly colocalizes with Gag patches at the plasma membrane, ΔCT Env forms small clusters throughout the membrane, with the majority of them situated at non-Gag sites. Nevertheless, some ΔCT Env can be found at budding sites, consistent with the fact that this mutant can be efficiently incorporated into HIV-1 virions produced in HeLa cells

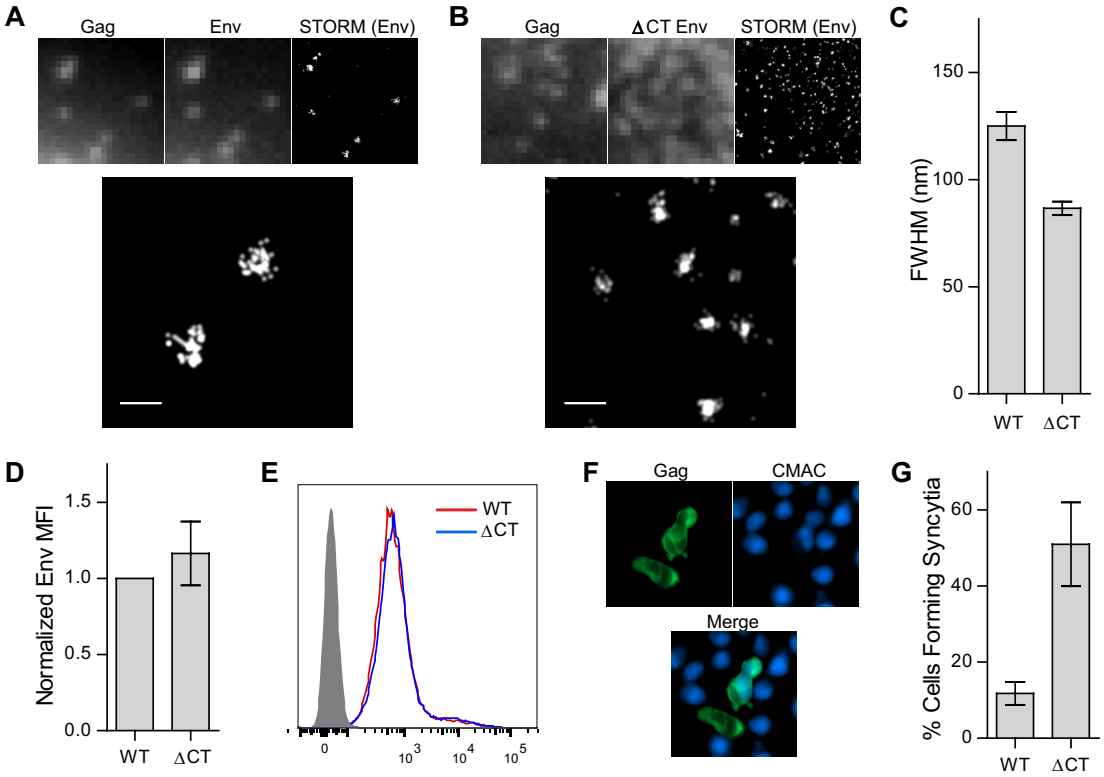

FIG 2 STORM imaging and fusion quantification of WT and ΔCT Env in infected T cells. (A, B) CEMss cells expressing either NL4-3 iGFP (A) or NL4-3 iGFP ΔCT (B) were subjected to STORM imaging. Scale bar = 200 nm. (C) Average of full width at half maximum (FWHM) measurements of individual Env clusters (±SEM, $n = 21$ WT Env, $n = 25$ ΔCT Env). CEMss cells were infected with NL4-3 iGFP or NL4-3 iGFP ΔCT and cultured for 48 h. Cells were then surface stained for Env and analyzed by flow cytometry. (D) Mean fluorescence intensities (MFI) of WT and ΔCT Env surface expression averaged from three separate experiments. (E) Representative histogram of surface Env levels. Shaded curve represents the mock condition. (F) After verification of equal surface Env levels, the infected cells were mixed at a 1:3 ratio with CMAC-labeled CEMss target cells for 3 h, fixed, and imaged. (G) Quantification of number of infected cells forming syncytia over 3 separate experiments (±standard deviation, $n = 308$ WT Env, $n = 313$ ΔCT Env).

(83). Interestingly, the ΔCT Env clusters at non-Gag sites were found to be significantly larger than the WT Env clusters outside assembly sites (~80 nm versus ~65 nm), documenting that the cytoplasmic domain is involved in regulating Env clustering. Also note that the size of ΔCT Env clusters at Gag sites did not differ from the size of Env clusters at non-Gag sites, strongly suggesting that Gag contributes to the Env clustering via an interaction with the Env cytoplasmic tail.

Much of the work dissecting HIV-1 assembly mechanisms has been done in adherent cells, such as 293T and HeLa cells, because they are more amenable to manipulation and imaging of protein sorting. Nevertheless, to confirm that the differences in clustering of WT and ΔCT Env that we observed in HeLa cells were mirrored in T cells, which are natural host cells for HIV-1, CEMss cells were infected with NL4-3 iGFP or NL4-3 iGFP ΔCT. These cells were then surface stained for Env, fixed, and subjected to STORM imaging. Because single budding sites are difficult to visualize at areas of dense Gag accumulation (50), we confined our analysis to individual budding sites in areas of sparser Gag fluorescence. Figure 2A to C document that, in T cells also, WT Env forms larger clusters than ΔCT Env at assembly sites, confirming the role of the Env CT in Gag-induced clustering.

The cytoplasmic tail regulates Env-induced fusion of producer and target cells. Presumably, the CT-dependent Env clustering at Gag sites (documented in Fig. 1 and 2A to C) evolved, at least partially, to guarantee the incorporation of Env into budding particles. Importantly, though, the Env CT has also been implicated in the maturation dependency of Env fusogenicity within free virions. Deletion of the CT rescues Env fusogenicity in immature particles and also allows Env trimers to accumulate where the particles contact the target cell membrane (14–16, 18). Our data shown in Figure 1 and 2A to C suggest that the restriction imposed by immature Gag on Env fusogenicity likely first takes place in the membrane of the producer cell and serves to prevent cell-cell fusion (i.e., the formation of syncytia) during cell-to-cell transmission events. To test this hypothesis, we infected CEMss cells with NL4-3 iGFP or NL4-3 iGFP ΔCT. Forty-eight hours postinfection, the cells were counted and mixed at a 1:3 ratio with CMAC-labeled target CEMss cells. The infection conditions were adjusted to render equal surface Env levels under each condition, as measured by flow cytometry over three separate experiments (Fig. 2D; a representative histogram is displayed in Figure 2E). After the cells were mixed, they were placed in the incubator for 3 h, fixed, and plated on MatTek dishes, and fields with 2 to 5 infected cells were imaged. Syncytia could be easily recognized by the presence of the blue CMAC within the green infected cells (Fig. 2F). Figure 2G displays the percentage of infected cells forming syncytia from 3 separate experiments. In total, 11.7% (36/308) of WT Env-expressing cells formed syncytia, while 50.5% (158/313) of ΔCT Env-expressing cells formed syncytia. Thus, the amount of Env-

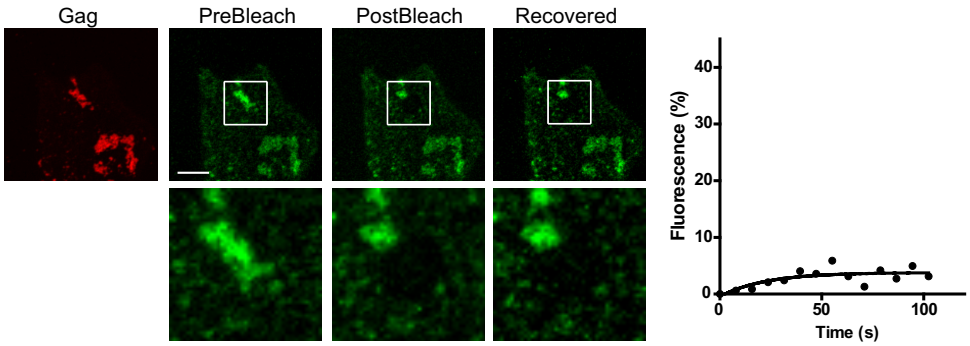

FIG 3 FRAP analysis of Env at assembly sites. FRAP was performed on Env at viral assembly sites. Blowups at bottom are of the respective boxed regions. Right, corresponding normalized recovery curve. Scale bar = 5 μm. Data are representative of 8 cells over 3 imaging sessions.

induced syncytium formation correlates inversely with the CT-dependent Gag-induced clustering of Env (observed in Fig. 1 and 2), strongly suggesting that Gag's interactions with the Env CT inhibit Env's ability to fuse membranes first when Env resides in the producer cell membrane and before virions are released.

Gag traps Env at assembly sites. The mobility of Env in the membrane may be important for its clustering capabilities and, ultimately, its ability to fuse viral and cellular membranes, as hypothesized in reference 18. Although this study suggests that Env mobility is important, so far it has not been possible to directly measure Env mobility in the viral membrane. However, techniques such as FRAP and fluorescence correlation spectroscopy (FCS) can be used to gather information on the mobility of proteins within the plasma membrane. Here, we employed FRAP to directly address the effects of the immature Gag lattice on Env mobility in live cells. We first focused on WT Env at Gag sites. HeLa cells were transfected with the proviral construct E-I-MA/p6 in which the Env gene is deleted (described in Materials and Methods), along with a WT Env expression plasmid (and Gag-mCherry to visualize budding sites). Sixteen to 20 h post-transfection, the cells were surface stained with anti-Env 2G12 Fab, followed by Fab-Alexa Fluor 488 secondary antibody. The FRAP imaging was performed as described in Materials and Methods. Photobleaching was confined to areas of Gag patching because the Env signal at non-Gag sites was very low and did not allow for the gathering of reliable recovery curves. As shown in Figure 3, WT Env showed no appreciable recovery at Gag sites in all cells tested ($n = 8$), confirming that WT Env is indeed trapped at Gag assembly sites.

Gag multimerization reduces the mobile fraction of ΔCT Env. Because truncation of the Env CT can relieve the fusion repression imposed by immature Gag both in virions (14–16, 18) and, as we now show, in cells (Fig. 2; also in HeLa cells, data not shown), we hypothesized that the mobility of ΔCT Env at assembly sites would correlate with the observed increase in Env-induced fusion. To evaluate the effects of Gag on ΔCT mobility, HeLa cells were transfected with E-I- MA/p6, ΔCT Env, and Gag-mCherry or a ΔCT Env expression plasmid alone. Sixteen to 20 h posttransfection, the cells were surface stained and imaged as described above. ΔCT Env in the absence of Gag (Fig. 4A) showed some level of recovery, with a mean diffusion coefficient of 0.0141 ± 0.001 $\mu m/s^2$ and a mobile fraction of 38.5% ± 2.1% ($n = 11$). When ΔCT Env was bleached at areas of Gag accumulation (Fig. 4B), the mean diffusion coefficient remained similar to that of ΔCT Env alone, 0 0.0143 ± 0 0.001 $\mu m/s^2$, but the mobile fraction was decreased to 27% ± 1.8% ($n = 11$) (Fig. 4E). Together with the results shown in Figures 2 and 3, these data demonstrate that, although Gag can restrict (to some degree) ΔCT Env mobility, the complete trapping of Env at budding sites is dependent on the Env CT and may account for its decreased fusogenicity.

Although ΔCT Env was still mobile at assembly sites, its mobility was restricted compared to that at non-Gag sites, suggesting that Gag multimerization can affect Env mobility even in the absence of a direct or indirect Gag-Env CT interaction. To test this, we utilized a multimerization-deficient Gag (monomeric Gag-cerulean) that can still bind to the plasma membrane (data not shown). Monomeric Gag and ΔCT Env expression constructs were cotransfected into HeLa cells, and the cells were labeled and imaged as described above (Fig. 4C). The average recovery curves from all cells tested are presented in Figure 4D. The mean diffusion coefficient of ΔCT Env in the presence of monomeric Gag (0.0187 ± 0.002 $\mu m/s^2$) was not significantly different from that of ΔCT Env alone or ΔCT Env in the presence of WT Gag (as measured by ANOVA; see Materials and Methods). Interestingly, the mobile fraction was calculated to be 36.5% ± 2.2% ($n = 11$), which is similar to the mobile fraction of ΔCT Env alone (38.5%) and significantly higher than the mobile fraction of ΔCT Env at Gag sites (27%) (Fig. 4E). Thus, Gag multimerization is required for the restriction of ΔCT Env mobility.

DISCUSSION

The clustering and organization of proteins and lipids in the plasma membrane is vital for membrane-based processes. A variety of interactions, most notably lipid-lipid, protein-lipid, and protein-protein interactions, have been described to contribute to the lateral organization of membrane domains (for a review, see reference 84). The HIV-1 Gag protein has recently been shown to reorganize preexisting membrane microdomains and to alter the dynamics of such domains (33, 34). Because the regulation of Env fusion is critical for efficient viral spread, we investigated how the presence of Gag affected the nanoscale organization and dynamics of Env in the plasma membrane. Our data revealed that Gag, at viral assembly sites, traps Env in a CT-dependent manner and that such trapping correlates with the inhibition of Env-induced fusion of producer and target cell membranes.

It is well established that Env forms trimers, with each subunit consisting of a heterodimeric complex formed by a surface subunit (gp120) and a transmembrane subunit (gp41). Using

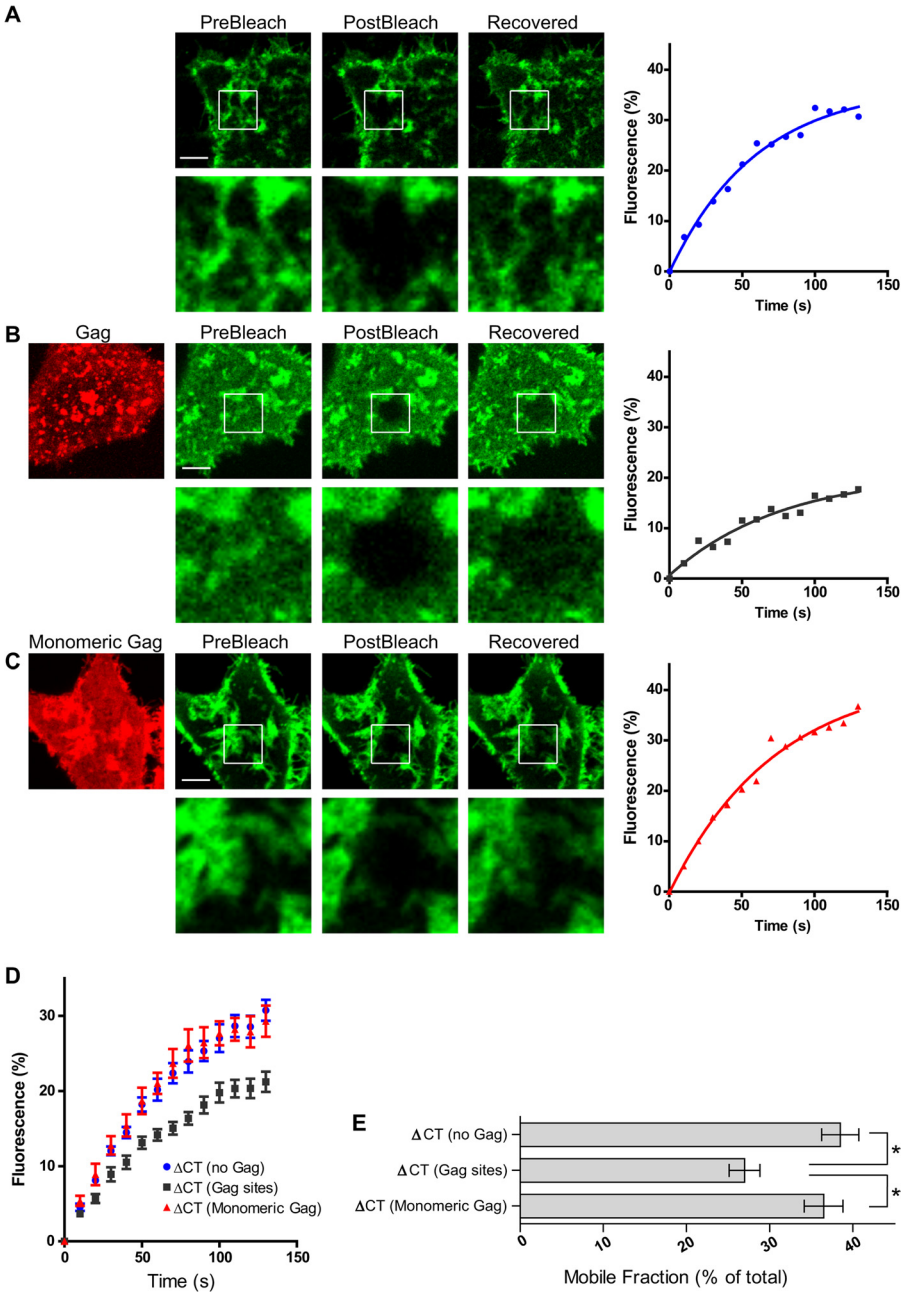

FIG 4 FRAP analysis of ΔCT Env. (A to C) FRAP was performed on ΔCT Env alone (A), with Gag (B), or with monomeric Gag (C). Right, corresponding normalized recovery curves. Scale bar = 5 μm. (D) Average recovery curves from all cells tested (±SEM, $n = 11$ for each condition). (E) Average mobile fraction for each condition (±SEM). For statistical analysis, a one-way ANOVA was performed with a Bonferroni *post hoc* test. Values were considered significantly different if the P value was ≤0.05.

STORM, we found that WT Env trimers form small clusters at the plasma membrane and that upon Gag assembly, these Env clusters become significantly larger, suggesting that the assembly process draws multiple small Env clusters to these sites. Although we cannot determine the stoichiometry of Env molecules in these clusters, previous work (high-pressure liquid chromatography [85] and electron tomography studies [86]) suggested that each nascent virion incorporates 7 to 21 Env trimers. Therefore, the small clusters we observed outside Gag assembly sites likely consisted of fewer than 7 trimers and perhaps as few as one. Note that, to some extent, the clustering of individual (or small groups of) Env trimers resembles the Gag-induced reorganization of tetraspanins and raft lipid-containing nanodomains mentioned above. It will be interesting to determine the sequence of recruitment of these and other host cell assemblages (for example, see reference 34), including the ones containing phosphatidylinositol-(4,5)-bisphosphate [PI(4,5)P_2], which has recently been shown to form discrete but very small domains (71).

Another superresolution study (53), which was in progress in parallel to the investigations presented here, also documents that

Env trimers cluster at Gag sites. In addition, both studies document that, unlike WT Env, ΔCT Env formed equal-size clusters throughout the plasma membrane that were not dependent on the presence of Gag. Thus, Gag apparently does not affect ΔCT Env clustering. Regarding the situation in viral particles, it was recently hypothesized that such differential accumulation of Env trimers is due to differences in Env mobility and, more specifically, that the immature Gag lattice inhibits Env from moving freely in the viral membrane. It was speculated that Env can form a single focus (consisting of multiple Env trimers) only upon particle maturation (i.e., Gag processing) because Env trimers then become mobile and can polarize toward the CD4 clusters on the target cell (18). However, directly measuring whether altered Env mobility is indeed responsible for altered accumulation of the viral fusogen cannot yet be done in viral particles as, to the best of our knowledge, no appropriate biophysical methods have been implemented to do that. Methods to analyze the mobility of integral membrane proteins in cellular membranes, however, are available, and we therefore set out, using FRAP, to measure the mobility of WT and ΔCT Env at Gag sites in the plasma membrane of producer cells. Our data demonstrate that the immature Gag lattice completely traps Env. Upon deletion of its CT, Env can move freely even at sites of Gag accumulation (i.e., at assembly/release sites), strongly suggesting that immature Gag traps Env via an interaction (direct or indirect) with the CT. The restoration of Env mobility (by deletion of the CT) was accompanied by a significant increase in Env-triggered cell-cell fusion, comparable to how CT deletion in particle-associated Env leads to a pronounced fusion increase for immature virions (14–16, 18). Our data thus strongly support the idea that the regulation of Env's mobility is linked with Env's ability to fuse membranes. Exactly how increased Env mobility (following CT deletion) ultimately results in increased fusion, however, remains to be analyzed. At a minimum, lateral Env mobility allows for the recruitment of multiple Env trimers to the site of interaction with CD4 (18, 19), i.e., it increases the likelihood that Env binds the receptor (and thus increases the likelihood that fusion is triggered). Additionally, the Gag maturation status and/or the presence of Env's CT likely also directly regulates the fusion process, either through modulating how Env and Gag interact with components of the cytoskeleton by regulating membrane stiffness (87), or perhaps, through changes that occur in the extracellular domain of Env. Studies have shown, for example, that Gag maturation and/or mutations in the CT, through a so-called "inside-out" mechanism, lead to changes in epitope exposure of gp120 (e.g., see references 88–91) and result in altered fusogenicity of Env.

Interestingly, while ΔCT Env, unlike WT Env, was still mobile at viral assembly sites, its mobility at those sites was reduced compared to its mobility elsewhere in the membrane. Also, the restriction of ΔCT Env mobility at assembly sites was dependent on Gag being able to multimerize. This finding is consistent with the hypothesis, recently put forward by Lucas et al., that the local accumulation of retroviral Gag creates a membrane environment that restricts Env glycoprotein mobility, perhaps facilitating Env incorporation into nascent particles (32). In that report, the authors measured how murine leukemia virus (MLV) and HIV-1 Gag competed for the acquisition of limited amounts of MLV Env. They documented that MLV Gag outcompeted HIV-1 Gag but, also, that the differences in incorporation decreased drastically if MLV Env was expressed without its cytoplasmic tail. Lucas et al. concluded that there are at least two mechanisms that allow for Env recruitment, a specific mechanism (which depends on Env's cytoplasmic domain) and a generic, tail-independent mechanism. Our FRAP data provide further support for the existence of such a generic mechanism, as they document that ΔCT Env mobility is restricted at sites of assembly. Together with the previously mentioned reports (33, 34), our data document that Gag multimerization, besides being obviously critical for particle morphogenesis, also adjusts the immediate membrane milieu, e.g., for the capturing of Env.

In summary, we have used superresolution microscopy in combination with live-cell analyses to define the clustering and dynamics of Env in the plasma membrane. Our results reveal nanoscale differences in Env clustering that correlate with Env's fusion activity. Regulation of this activity is critical: a substantial amount of Env at the plasma membrane does not get incorporated into particles (53; also data not shown). While Env situated adjacent to budding sites has been hypothesized to promote the formation and maintenance of the virological synapse (VS) (53), if unhindered by Gag, host cell proteins, and/or restrictions imposed by the topology of membrane areas where Env is situated, Env would likely trigger the fusion of producer and target cells, thus leading to the formation of syncytia. Some syncytium formation may be tolerable or (under certain circumstances) even beneficial for virus spread, as evidenced by *in vitro* analyses, as well as a recent study of the migration of infected cells in lymph nodes of humanized mice (13, 92, 93). The latter study, however, also documented that only a small subset of infected lymphocytes fused to form syncytia, suggesting that the virus evolved mechanisms that allow it to prevent excessive formation of these multinucleated entities.

ACKNOWLEDGMENTS

We thank the UVM Microscopy Imaging Facility for use of both the Nikon N-STORM microscope and the Zeiss 510 Meta confocal microscope. We thank Christopher Huston for filter cubes and useful discussions and the laboratory of Gary Ward for reagents (special thanks to Anne Kelsen). We acknowledge the following researchers for their contribution of reagents: Marc Johnson for the WT and ΔCT Env expression vectors, Eric Freed for the pNL4-3 EnvΔCT provirus, Michael Kay for the E-I- MA/p6 proviral construct, Paul Spearman for both GagGFP and monomeric Gag-cerulean, and Paul Bieniasz for the Gag-mCherry construct. Hans-Georg Kräusslich is acknowledged for discussing with us some of his group's unpublished results. Finally, we thank Alan Howe, Gary Ward, Jason Botten, and Menelaos Symeonides for critical reading of the manuscript.

Support for this work was provided by NIH grant R01 AI080302 to M.T. and training grant T32 AI055402-06A1 to N.H.R.

REFERENCES

1. **Grove J, Marsh M.** 2011. The cell biology of receptor-mediated virus entry. J. Cell Biol. **195**:1071–1082.
2. **Sattentau Q.** 2008. Avoiding the void: cell-to-cell spread of human viruses. Nat. Rev. Microbiol. **6**:815–826.
3. **Zhong P, Agosto LM, Munro JB, Mothes W.** 2013. Cell-to-cell transmission of viruses. Curr. Opin. Virol. **3**:44–50.
4. **Sato H, Orenstein J, Dimitrov D, Martin M.** 1992. Cell-to-cell spread of HIV-1 occurs within minutes and may not involve the participation of virus particles. Virology **186**:712–724.
5. **Dimitrov DS, Willey RL, Sato H, Chang LJ, Blumenthal R, Martin MA.** 1993. Quantitation of human immunodeficiency virus type 1 infection kinetics. J. Virol. **67**:2182–2190.
6. **Tan X, Pearce-Pratt R, Phillips DM.** 1993. Productive infection of a cervical epithelial cell line with human immunodeficiency virus: implications for sexual transmission. J. Virol. **67**:6447–6452.

7. **Cheynier R, Henrichwark S, Hadida F, Pelletier E, Oksenhendler E, Autran B, Wain-Hobson S.** 1994. HIV and T cell expansion in splenic white pulps is accompanied by infiltration of HIV-specific cytotoxic T lymphocytes. Cell **78**:373–387.
8. **McDonald D, Wu L, Bohks SM, KewalRamani VN, Unutmaz D, Hope TJ.** 2003. Recruitment of HIV and its receptors to dendritic cell-T cell junctions. Science **300**:1295–1297.
9. **Jolly C, Kashefi K, Hollinshead M, Sattentau QJ.** 2004. HIV-1 cell to cell transfer across an Env-induced, actin-dependent synapse. J. Exp. Med. **199**:283–293.
10. **Chen P, Hubner W, Spinelli MA, Chen BK.** 2007. Predominant mode of human immunodeficiency virus transfer between T cells is mediated by sustained Env-dependent neutralization-resistant virological synapses. J. Virol. **81**:12582–12595.
11. **Sourisseau M, Sol-Foulon N, Porrot F, Blanchet F, Schwartz O.** 2007. Inefficient human immunodeficiency virus replication in mobile lymphocytes. J. Virol. **81**:1000–1012.
12. **Hubner W, McNerney GP, Chen P, Dale BM, Gordon RE, Chuang FY, Li XD, Asmuth DM, Huser T, Chen BK.** 2009. Quantitative 3D video microscopy of HIV transfer across T cell virological synapses. Science **323**:1743–1747.
13. **Murooka TT, Deruaz M, Marangoni F, Vrbanac VD, Seung E, von Andrian UH, Tager AM, Luster AD, Mempel TR.** 2012. HIV-infected T cells are migratory vehicles for viral dissemination. Nature **490**:283–287.
14. **Murakami T, Ablan S, Freed EO, Tanaka Y.** 2004. Regulation of human immunodeficiency virus type 1 Env-mediated membrane fusion by viral protease activity. J. Virol. **78**:1026–1031.
15. **Wyma DJ, Jiang J, Shi J, Zhou J, Lineberger JE, Miller MD, Aiken C.** 2004. Coupling of human immunodeficiency virus type 1 fusion to virion maturation: a novel role of the gp41 cytoplasmic tail. J. Virol. **78**:3429–3435.
16. **Jiang J, Aiken C.** 2007. Maturation-dependent human immunodeficiency virus type 1 particle fusion requires a carboxyl-terminal region of the gp41 cytoplasmic tail. J. Virol. **81**:9999–10008.
17. **Sundquist WI, Krausslich HG.** 2012. HIV-1 assembly, budding, and maturation. Cold Spring Harb. Perspect. Med. **2**:a006924. doi:10.1101/cshperspect.a006924.
18. **Chojnacki J, Staudt T, Glass B, Bingen P, Engelhardt J, Anders M, Schneider J, Muller B, Hell SW, Krausslich HG.** 2012. Maturation-dependent HIV-1 surface protein redistribution revealed by fluorescence nanoscopy. Science **338**:524–528.
19. **Sougrat R, Bartesaghi A, Lifson JD, Bennett AE, Bess JW, Zabransky DJ, Subramaniam S.** 2007. Electron tomography of the contact between T cells and SIV/HIV-1: implications for viral entry. PLoS Pathog. **3**:e63. doi:10.1371/journal.ppat.0030063.
20. **Yu X, Yuan X, Matsuda Z, Lee TH, Essex M.** 1992. The matrix protein of human immunodeficiency virus type 1 is required for incorporation of viral envelope protein into mature virions. J. Virol. **66**:4966–4971.
21. **Dorfman T, Mammano F, Haseltine WA, Gottlinger HG.** 1994. Role of the matrix protein in the virion association of the human immunodeficiency virus type 1 envelope glycoprotein. J. Virol. **68**:1689–1696.
22. **Freed EO, Orenstein JM, Buckler-White AJ, Martin MA.** 1994. Single amino acid changes in the human immunodeficiency virus type 1 matrix protein block virus particle production. J. Virol. **68**:5311–5320.
23. **Freed EO, Martin MA.** 1995. Virion incorporation of envelope glycoproteins with long but not short cytoplasmic tails is blocked by specific, single amino acid substitutions in the human immunodeficiency virus type 1 matrix. J. Virol. **69**:1984–1989.
24. **Freed EO, Martin MA.** 1996. Domains of the human immunodeficiency virus type 1 matrix and gp41 cytoplasmic tail required for envelope incorporation into virions. J. Virol. **70**:341–351.
25. **Murakami T, Freed EO.** 2000. Genetic evidence for an interaction between human immunodeficiency virus type 1 matrix and alpha-helix 2 of the gp41 cytoplasmic tail. J. Virol. **74**:3548–3554.
26. **Akari H, Fukumori T, Adachi A.** 2000. Cell-dependent requirement of human immunodeficiency virus type 1 gp41 cytoplasmic tail for Env incorporation into virions. J. Virol. **74**:4891–4893.
27. **Brandano L, Stevenson M.** 2012. A highly conserved residue in the C-terminal helix of HIV-1 matrix is required for envelope incorporation into virus particles. J. Virol. **86**:2347–2359.
28. **Checkley MA, Luttge BG, Freed EO.** 2011. HIV-1 envelope glycoprotein biosynthesis, trafficking, and incorporation. J. Mol. Biol. **410**:582–608.
29. **Mammano F, Kondo E, Sodroski J, Bukovsky A, Gottlinger HG.** 1995. Rescue of human immunodeficiency virus type 1 matrix protein mutants by envelope glycoproteins with short cytoplasmic domains. J. Virol. **69**:3824–3830.
30. **Reil H, Bukovsky AA, Gelderblom HR, Gottlinger HG.** 1998. Efficient HIV-1 replication can occur in the absence of the viral matrix protein. EMBO J. **17**:2699–2708.
31. **Johnson MC.** 2011. Mechanisms for Env glycoprotein acquisition by retroviruses. AIDS Res. Hum. Retroviruses **27**:239–247.
32. **Lucas TM, Lyddon TD, Grosse SA, Johnson MC.** 2010. Two distinct mechanisms regulate recruitment of murine leukemia virus envelope protein to retroviral assembly sites. Virology **405**:548–555.
33. **Krementsov DN, Rassam P, Margeat E, Roy NH, Schneider-Schaulies J, Milhiet PE, Thali M.** 2010. HIV-1 assembly differentially alters dynamics and partitioning of tetraspanins and raft components. Traffic **11**:1401–1414.
34. **Hogue IB, Grover JR, Soheilian F, Nagashima K, Ono A.** 2011. Gag induces the coalescence of clustered lipid rafts and tetraspanin-enriched microdomains at HIV-1 assembly sites on the plasma membrane. J. Virol. **85**:9749–9766.
35. **Waheed AA, Freed EO.** 2009. Lipids and membrane microdomains in HIV-1 replication. Virus Res. **143**:162–176.
36. **Ono A.** 2010. Relationships between plasma membrane microdomains and HIV-1 assembly. Biol. Cell **102**:335–350.
37. **Gomez CY, Hope TJ.** 2006. Mobility of human immunodeficiency virus type 1 Pr55Gag in living cells. J. Virol. **80**:8796–8806.
38. **Jouvenet N, Bieniasz PD, Simon SM.** 2008. Imaging the biogenesis of individual HIV-1 virions in live cells. Nature **454**:236–240.
39. **Ivanchenko S, Godinez WJ, Lampe M, Krausslich HG, Eils R, Rohr K, Brauchle C, Muller B, Lamb DC.** 2009. Dynamics of HIV-1 assembly and release. PLoS Pathog. **5**:e1000652. doi:10.1371/journal.ppat.1000652.
40. **Jouvenet N, Simon SM, Bieniasz PD.** 2009. Imaging the interaction of HIV-1 genomes and Gag during assembly of individual viral particles. Proc. Natl. Acad. Sci. U. S. A. **106**:19114–19119.
41. **Kemler I, Meehan A, Poeschla EM.** 2010. Live-cell coimaging of the genomic RNAs and Gag proteins of two lentiviruses. J. Virol. **84**:6352–6366.
42. **Baumgartel V, Ivanchenko S, Dupont A, Sergeev M, Wiseman PW, Krausslich HG, Brauchle C, Muller B, Lamb DC.** 2011. Live-cell visualization of dynamics of HIV budding site interactions with an ESCRT component. Nat. Cell Biol. **13**:469–474.
43. **Jouvenet N, Zhadina M, Bieniasz PD, Simon SM.** 2011. Dynamics of ESCRT protein recruitment during retroviral assembly. Nat. Cell Biol. **13**:394–401.
44. **Betzig E, Patterson GH, Sougrat R, Lindwasser OW, Olenych S, Bonifacino JS, Davidson MW, Lippincott-Schwartz J, Hess HF.** 2006. Imaging intracellular fluorescent proteins at nanometer resolution. Science **313**:1642–1645.
45. **Lelek M, Di Nunzio F, Henriques R, Charneau P, Arhel N, Zimmer C.** 2012. Superresolution imaging of HIV in infected cells with FlAsH-PALM. Proc. Natl. Acad. Sci. U. S. A. **109**:8564–8569.
46. **Pereira CF, Rossy J, Owen DM, Mak J, Gaus K.** 2012. HIV taken by STORM: super-resolution fluorescence microscopy of a viral infection. Virol. J. **9**:84. doi:10.1186/1743-422X-9-84.
47. **Manley S, Gillette JM, Patterson GH, Shroff H, Hess HF, Betzig E, Lippincott-Schwartz J.** 2008. High-density mapping of single-molecule trajectories with photoactivated localization microscopy. Nat. Methods **5**:155–157.
48. **Eckhardt M, Anders M, Muranyi W, Heilemann M, Krijnse-Locker J, Muller B.** 2011. A SNAP-tagged derivative of HIV-1—a versatile tool to study virus-cell interactions. PLoS One **6**:e22007. doi:10.1371/journal.pone.0022007.
49. **Gunzenhauser J, Olivier N, Pengo T, Manley S.** 2012. Quantitative super-resolution imaging reveals protein stoichiometry and nanoscale morphology of assembling HIV-Gag virions. Nano Lett. **12**:4705–4710.
50. **Malkusch S, Muranyi W, Muller B, Krausslich HG, Heilemann M.** 2013. Single-molecule coordinate-based analysis of the morphology of HIV-1 assembly sites with near-molecular spatial resolution. Histochem. Cell Biol. **139**:173–179.
51. **Gaudin R, Cunha de Alencar B, Jouve M, Berre S, Le Bouder E, Schindler M, Varthaman A, Gobert FX, Benaroch P.** 2012. Critical role for the kinesin KIF3A in the HIV life cycle in primary human macrophages. J. Cell Biol. **199**:467–479.
52. **Lehmann M, Rocha S, Mangeat B, Blanchet F, Uji IH, Hofkens J, Piguet**

V. 2011. Quantitative multicolor super-resolution microscopy reveals tetherin HIV-1 interaction. PLoS Pathog. **7**:e1002456. doi:10.1371/journal.ppat.1002456.
53. **Muranyi W, Malkusch S, Muller B, Heilemann M, Krausslich HG.** 2013. Super-resolution microscopy reveals specific recruitment of HIV-1 envelope proteins to viral assembly sites dependent on the envelope C-terminal tail. PLoS Pathog. **9**:e1003198. doi:10.1371/journal.ppat.1003198.
54. **Larson DR, Johnson MC, Webb WW, Vogt VM.** 2005. Visualization of retrovirus budding with correlated light and electron microscopy. Proc. Natl. Acad. Sci. U. S. A. **102**:15453–15458.
55. **Jorgenson RL, Vogt VM, Johnson MC.** 2009. Foreign glycoproteins can be actively recruited to virus assembly sites during pseudotyping. J. Virol. **83**:4060–4067.
56. **Hubner W, Chen P, Del Portillo A, Liu Y, Gordon RE, Chen BK.** 2007. Sequence of human immunodeficiency virus type 1 (HIV-1) Gag localization and oligomerization monitored with live confocal imaging of a replication-competent, fluorescently tagged HIV-1. J. Virol. **81**:12596–12607.
57. **Dou J, Wang JJ, Chen X, Li H, Ding L, Spearman P.** 2009. Characterization of a myristoylated, monomeric HIV Gag protein. Virology **387**:341–352.
58. **Kiskowski MA, Hancock JF, Kenworthy AK.** 2009. On the use of Ripley's K-function and its derivatives to analyze domain size. Biophys. J. **97**:1095–1103.
59. **Veatch SL, Machta BB, Shelby SA, Chiang EN, Holowka DA, Baird BA.** 2012. Correlation functions quantify super-resolution images and estimate apparent clustering due to over-counting. PLoS One **7**:e31457. doi:10.1371/journal.pone.0031457.
60. **Snapp EL, Altan N, Lippincott-Schwartz J.** 2003. Measuring protein mobility by photobleaching GFP chimeras in living cells. Curr. Protoc. Cell Biol. **Chap 21**:Unit 21.21.
61. **Axelrod D, Koppel DE, Schlessinger J, Elson E, Webb WW.** 1976. Mobility measurement by analysis of fluorescence photobleaching recovery kinetics. Biophys. J. **16**:1055–1069.
62. **Soumpasis DM.** 1983. Theoretical analysis of fluorescence photobleaching recovery experiments. Biophys. J. **41**:95–97.
63. **Hess ST, Gould TJ, Gudheti MV, Maas SA, Mills KD, Zimmerberg J.** 2007. Dynamic clustered distribution of hemagglutinin resolved at 40 nm in living cell membranes discriminates between raft theories. Proc. Natl. Acad. Sci. U. S. A. **104**:17370–17375.
64. **Kellner RR, Baier CJ, Willig KI, Hell SW, Barrantes FJ.** 2007. Nanoscale organization of nicotinic acetylcholine receptors revealed by stimulated emission depletion microscopy. Neuroscience **144**:135–143.
65. **Sieber JJ, Willig KI, Kutzner C, Gerding-Reimers C, Harke B, Donnert G, Rammner B, Eggeling C, Hell SW, Grubmuller H, Lang T.** 2007. Anatomy and dynamics of a supramolecular membrane protein cluster. Science **317**:1072–1076.
66. **Huang B, Wang W, Bates M, Zhuang X.** 2008. Three-dimensional super-resolution imaging by stochastic optical reconstruction microscopy. Science **319**:810–813.
67. **Eggeling C, Ringemann C, Medda R, Schwarzmann G, Sandhoff K, Polyakova S, Belov VN, Hein B, von Middendorff C, Schonle A, Hell SW.** 2009. Direct observation of the nanoscale dynamics of membrane lipids in a living cell. Nature **457**:1159–1162.
68. **Lillemeier BF, Mortelmaier MA, Forstner MB, Huppa JB, Groves JT, Davis MM.** 2010. TCR and Lat are expressed on separate protein islands on T cell membranes and concatenate during activation. Nat. Immunol. **11**:90–96.
69. **Owen DM, Rentero C, Rossy J, Magenau A, Williamson D, Rodriguez M, Gaus K.** 2010. PALM imaging and cluster analysis of protein heterogeneity at the cell surface. J. Biophotonics **3**:446–454.
70. **Sengupta P, Jovanovic-Talisman T, Skoko D, Renz M, Veatch SL, Lippincott-Schwartz J.** 2011. Probing protein heterogeneity in the plasma membrane using PALM and pair correlation analysis. Nat. Methods **8**:969–975.
71. **van den Bogaart G, Meyenberg K, Risselada HJ, Amin H, Willig KI, Hubrich BE, Dier M, Hell SW, Grubmuller H, Diederichsen U, Jahn R.** 2011. Membrane protein sequestering by ionic protein-lipid interactions. Nature **479**:552–555.
72. **Bar-On D, Wolter S, van de Linde S, Heilemann M, Nudelman G, Nachliel E, Gutman M, Sauer M, Ashery U.** 2012. Super-resolution imaging reveals the internal architecture of nano-sized syntaxin clusters. J. Biol. Chem. **287**:27158–27167.
73. **Itano MS, Steinhauer C, Schmied JJ, Forthmann C, Liu P, Neumann AK, Thompson NL, Tinnefeld P, Jacobson K.** 2012. Super-resolution imaging of C-type lectin and influenza hemagglutinin nanodomains on plasma membranes using blink microscopy. Biophys. J. **102**:1534–1542.
74. **Rossy J, Owen DM, Williamson DJ, Yang Z, Gaus K.** 2013. Conformational states of the kinase Lck regulate clustering in early T cell signaling. Nat. Immunol. **14**:82–89.
75. **Ripley BD.** 1977. Modelling spatial patterns. J. R. Stat. Soc. **39**:172–212.
76. **Ripley BD.** 1979. Tests of 'randomness' for spatial point patterns. J. R. Stat. Soc. **41**:368–374.
77. **Rowell JF, Stanhope PE, Siliciano RF.** 1995. Endocytosis of endogenously synthesized HIV-1 envelope protein. Mechanism and role in processing for association with class II MHC. J. Immunol. **155**:473–488.
78. **Egan MA, Carruth LM, Rowell JF, Yu X, Siliciano RF.** 1996. Human immunodeficiency virus type 1 envelope protein endocytosis mediated by a highly conserved intrinsic internalization signal in the cytoplasmic domain of gp41 is suppressed in the presence of the Pr55gag precursor protein. J. Virol. **70**:6547–6556.
79. **Ohno H, Aguilar RC, Fournier MC, Hennecke S, Cosson P, Bonifacino JS.** 1997. Interaction of endocytic signals from the HIV-1 envelope glycoprotein complex with members of the adaptor medium chain family. Virology **238**:305–315.
80. **Boge M, Wyss S, Bonifacino JS, Thali M.** 1998. A membrane-proximal tyrosine-based signal mediates internalization of the HIV-1 envelope glycoprotein via interaction with the AP-2 clathrin adaptor. J. Biol. Chem. **273**:15773–15778.
81. **Berlioz-Torrent C, Shacklett BL, Erdtmann L, Delamarre L, Bouchaert I, Sonigo P, Dokhelar MC, Benarous R.** 1999. Interactions of the cytoplasmic domains of human and simian retroviral transmembrane proteins with components of the clathrin adaptor complexes modulate intracellular and cell surface expression of envelope glycoproteins. J. Virol. **73**:1350–1361.
82. **Byland R, Vance PJ, Hoxie JA, Marsh M.** 2007. A conserved dileucine motif mediates clathrin and AP-2-dependent endocytosis of the HIV-1 envelope protein. Mol. Biol. Cell **18**:414–425.
83. **Murakami T, Freed EO.** 2000. The long cytoplasmic tail of gp41 is required in a cell type-dependent manner for HIV-1 envelope glycoprotein incorporation into virions. Proc. Natl. Acad. Sci. U. S. A. **97**:343–348.
84. **Lingwood D, Simons K.** 2010. Lipid rafts as a membrane-organizing principle. Science **327**:46–50.
85. **Chertova E, Bess JW, Jr, Crise BJ, Sowder IR, Schaden TM, Hilburn JM, Hoxie JA, Benveniste RE, Lifson JD, Henderson LE, Arthur LO.** 2002. Envelope glycoprotein incorporation, not shedding of surface envelope glycoprotein (gp120/SU), is the primary determinant of SU content of purified human immunodeficiency virus type 1 and simian immunodeficiency virus. J. Virol. **76**:5315–5325.
86. **Zhu P, Liu J, Bess J, Jr, Chertova E, Lifson JD, Grise H, Ofek GA, Taylor KA, Roux KH.** 2006. Distribution and three-dimensional structure of AIDS virus envelope spikes. Nature **441**:847–852.
87. **Kol N, Shi Y, Tsvitov M, Barlam D, Shneck RZ, Kay MS, Rousso I.** 2007. A stiffness switch in human immunodeficiency virus. Biophys. J. **92**:1777–1783.
88. **Edwards TG, Wyss S, Reeves JD, Zolla-Pazner S, Hoxie JA, Doms RW, Baribaud F.** 2002. Truncation of the cytoplasmic domain induces exposure of conserved regions in the ectodomain of human immunodeficiency virus type 1 envelope protein. J. Virol. **76**:2683–2691.
89. **Kalia V, Sarkar S, Gupta P, Montelaro RC.** 2005. Antibody neutralization escape mediated by point mutations in the intracytoplasmic tail of human immunodeficiency virus type 1 gp41. J. Virol. **79**:2097–2107.
90. **Wyss S, Dimitrov AS, Baribaud F, Edwards TG, Blumenthal R, Hoxie JA.** 2005. Regulation of human immunodeficiency virus type 1 envelope glycoprotein fusion by a membrane-interactive domain in the gp41 cytoplasmic tail. J. Virol. **79**:12231–12241.
91. **Joyner AS, Willis JR, Crowe JE, Jr, Aiken C.** 2011. Maturation-induced cloaking of neutralization epitopes on HIV-1 particles. PLoS Pathog. **7**:e1002234. doi:10.1371/journal.ppat.1002234.
92. **Sylwester A, Murphy S, Shutt D, Soll DR.** 1997. HIV-induced T cell syncytia are self-perpetuating and the primary cause of T cell death in culture. J. Immunol. **158**:3996–4007.
93. **Shutt DC, Jenkins LM, Carolan EJ, Stapleton J, Daniels KJ, Kennedy RC, Soll DR.** 1998. T cell syncytia induced by HIV release. T cell chemoattractants: demonstration with a newly developed single cell chemotaxis chamber. J. Cell Sci. **111**(Pt 1):99–109.